articles

molecular pharmaceutics

Effects of pH and Polyanions on the Thermal Stability of Fibroblast Growth Factor 20

Haihong Fan,[†] Samadhi N. Vitharana,[†] Tracy Chen,[‡] Donald O'Keefe,[‡] and C. Russell Middaugh*,[†]

Department of Pharmaceutical Chemistry, University of Kansas, 2030 Becker Drive, Lawrence, Kansas 66044, and CuraGen Corporation, Branford, Connecticut 06405

Received September 11, 2006; Revised Manuscript Received October 23, 2006; Accepted November 16, 2006

Abstract: Fibroblast growth factor 20 (FGF20) is a member of the FGF family with potential for use in several different therapeutic categories. In this work, we provide the first structural characterization of FGF20 using a wide variety of approaches. Like other members of the FGF family, FGF20 appears to possess a β-trefoil structure. The effect of pH on the conformation and thermal stability of FGF20 is evaluated using far-UV circular dichroism (CD), intrinsic and ANS fluorescence, and high-resolution derivative UV absorption spectroscopy. Empirical phase diagrams are constructed to describe the solution behavior of FGF20 over a wide pH and temperature range. The protein appears to be unstable at pH <5, with aggregation and precipitation observed during dialysis. A major heat-induced conformational change also causes aggregation and precipitation of FGF20 at elevated temperatures. The highest thermal stability is observed near neutral pH ($T_m \sim 55$ °C at pH 7). The effect of several high- and low-molecular mass polyanions on the thermal stability of FGF20 is also examined using CD, intrinsic fluorescence, and DSC analysis. Among these ligands, heparin exhibits the greatest stabilizing effect on FGF20, increasing the T_m by more than 10 °C.

Keywords: Fibroblast growth factor; thermal stability; circular dichroism; fluorescence spectroscopy; absorption spectroscopy; differential scanning calorimetry; empirical phase diagram

Introduction

Fibroblast growth factors (FGFs) constitute a large family of structurally related proteins involved in a variety of physiological, developmental, and pathological processes. The FGF family consists of at least 22 members, exhibiting distinct spatial and temporal expression patterns. Most FGFs (except FGF11−FGF14) are either constitutively secreted or transported in an unspecified manner to the extracellular space.[1] Secreted FGFs bind to several tyrosine kinase receptors (FGFR) on the cell surface. The binding subsequently initiates the FGFR signal transduction pathway, which has been implicated in the regulation of various developmental events. Interactions between the FGFs and their receptors are regulated by heparan sulfate proteoglycans found on cell surfaces in the extracellular matrix.[2]

Several members of the FGF family have been shown to exhibit only marginal stability under physiological conditions.[3,4] For example, a molten globule-like state of FGF1 has been observed in the physiological temperature range with disrupted tertiary structure, while its native secondary structure is maintained.[5] It has been suggested that this

* To whom correspondence should be addressed: Department of Pharmaceutical Chemistry, University of Kansas, 2030 Becker Drive, Lawrence, KS 66044. Telephone: (785) 864-5813. Fax: (785) 864-5814. E-mail: middaugh@ku.edu.

[†] University of Kansas.

[‡] CuraGen Corp.

(1) Ornitz, D. M.; Itoh, N. Fibroblast growth factors. *Genome Biol.* **2001**, *2* (3), REVIEWS3005.

(2) Ornitz, D. M. FGFs, heparan sulfate and FGFRs: Complex interactions essential for development. *BioEssays* **2000**, *22* (2), 108−12.

(3) Chen, B. L.; Arakawa, T.; Morris, C. F.; Kenney, W. C.; Wells, C. M.; Pitt, C. G. Aggregation pathway of recombinant human keratinocyte growth factor and its stabilization. *Pharm. Res.* **1994**, *11* (11), 1581−7.

10.1021/mp060097h CCC: $37.00
Published on Web 01/03/2007

partially unfolded state of FGF1 is involved in an ability to translocate through cell membranes without a conventional signal sequence.[6,7] In some cases, polyanions such as heparin and heparan sulfate can bind to FGF proteins and lock the molecules in their native conformations, protecting them from thermal unfolding as well as oxidative, proteolytic, and acidic conditions.[8−11] Besides polyanions, general protein stabilizers such as sugars and amino acids have also been shown to exhibit significant stabilizing effects on FGFs.[12,13]

FGF20 is a member of the FGF family preferentially expressed in the substantia nigra of the brain.[14−16] It shows neurotrophic effects for dopaminergic neurons in the substantia nigra and may therefore be important in the treatment of neurodegenerative pathologies such as Parkinson's disease.[17,18] The therapeutic potential of FGF20 has also been explored for the treatment of acute intestinal inflammation and chemotherapy-induced oral mucositis.[19,20] Among the members of FGF family, FGF9 has the highest degree of amino acid sequence homology (70%) with FGF20.[16] The crystal structure of FGF9 has been determined,[21] revealing a core structure of a β-trefoil fold which is preserved in the FGF family.[22,23] It exists in cells as a dimer, which is formed by interactions of the N- and C-terminal regions outside the β-trefoil core. Potential heparin binding sites were also identified on the surface of the protein. For FGF20, however, no structural characterization or stability information has been previously reported in literature, although the sequence is known.[14−16]

The primary goal of this work is to provide a structural characterization of FGF20 using a variety of biophysical tools. The quaternary, tertiary, and secondary structure of the protein is characterized over a wide pH and temperature range using primarily spectroscopic techniques such as high-resolution UV absorption spectroscopy, intrinsic and extrinsic fluorescence, and far-UV circular dichroism (CD). The results are summarized using an empirical phase diagram approach described previously.[24,25] The effects of representa-

(4) Copeland, R. A.; Ji, H.; Halfpenny, A. J.; Williams, R. W.; Thompson, K. C.; Herber, W. K.; Thomas, K. A.; Bruner, M. W.; Ryan, J. A.; Marquis-Omer, D.; et al. The structure of human acidic fibroblast growth factor and its interaction with heparin. *Arch. Biochem. Biophys.* **1991**, *289* (1), 53−61.

(5) Mach, H.; Ryan, J. A.; Burke, C. J.; Volkin, D. B.; Middaugh, C. R. Partially structured self-associating states of acidic fibroblast growth factor. *Biochemistry* **1993**, *32* (30), 7703−11.

(6) Edwards, K. L.; Kueltzo, L. A.; Fisher, M. T.; Middaugh, C. R. Complex effects of molecular chaperones on the aggregation and refolding of fibroblast growth factor-1. *Arch. Biochem. Biophys.* **2001**, *393* (1), 14−21.

(7) Mach, H.; Middaugh, C. R. Interaction of partially structured states of acidic fibroblast growth factor with phospholipid membranes. *Biochemistry* **1995**, *34* (31), 9913−20.

(8) Vemuri, S.; Beylin, I.; Sluzky, V.; Stratton, P.; Eberlein, G.; Wang, Y. J. The stability of bFGF against thermal denaturation. *J. Pharm. Pharmacol.* **1994**, *46* (6), 481−6.

(9) Linemeyer, D. L.; Menke, J. G.; Kelly, L. J.; DiSalvo, J.; Soderman, D.; Schaeffer, M. T.; Ortega, S.; Gimenez-Gallego, G.; Thomas, K. A. Disulfide bonds are neither required, present, nor compatible with full activity of human recombinant acidic fibroblast growth factor. *Growth Factors* **1990**, *3* (4), 287−98.

(10) Rosengart, T. K.; Johnson, W. V.; Friesel, R.; Clark, R.; Maciag, T. Heparin protects heparin-binding growth factor-I from proteolytic inactivation in vitro. *Biochem. Biophys. Res. Commun.* **1988**, *152* (1), 432−40.

(11) Gospodarowicz, D.; Cheng, J. Heparin protects basic and acidic FGF from inactivation. *J. Cell. Physiol.* **1986**, *128* (3), 475−84.

(12) Chen, B. L.; Arakawa, T. Stabilization of recombinant human keratinocyte growth factor by osmolytes and salts. *J. Pharm. Sci.* **1996**, *85* (4), 419−26.

(13) Tsai, P. K.; Volkin, D. B.; Dabora, J. M.; Thompson, K. C.; Bruner, M. W.; Gress, J. O.; Matuszewska, B.; Keogan, M.; Bondi, J. V.; Middaugh, C. R. Formulation design of acidic fibroblast growth factor. *Pharm. Res.* **1993**, *10* (5), 649−59.

(14) Jeffers, M.; Shimkets, R.; Prayaga, S.; Boldog, F.; Yang, M.; Burgess, C.; Fernandes, E.; Rittman, B.; Shimkets, J.; LaRochelle, W. J.; Lichenstein, H. S. Identification of a novel human fibroblast growth factor and characterization of its role in oncogenesis. *Cancer Res.* **2001**, *61* (7), 3131−8.

(15) Ohmachi, S.; Watanabe, Y.; Mikami, T.; Kusu, N.; Ibi, T.; Akaike, A.; Itoh, N. FGF-20, a novel neurotrophic factor, preferentially expressed in the substantia nigra pars compacta of rat brain. *Biochem. Biophys. Res. Commun.* **2000**, *277* (2), 355−60.

(16) Kirikoshi, H.; Sagara, N.; Saitoh, T.; Tanaka, K.; Sekihara, H.; Shiokawa, K.; Katoh, M. Molecular cloning and characterization of human FGF-20 on chromosome 8p21.3-p22. *Biochem. Biophys. Res. Commun.* **2000**, *274* (2), 337−43.

(17) van der Walt, J. M.; Noureddine, M. A.; Kittappa, R.; Hauser, M. A.; Scott, W. K.; McKay, R.; Zhang, F.; Stajich, J. M.; Fujiwara, K.; Scott, B. L.; Pericak-Vance, M. A.; Vance, J. M.; Martin, E. R. Fibroblast growth factor 20 polymorphisms and haplotypes strongly influence risk of Parkinson disease. *Am. J. Hum. Genet.* **2004**, *74* (6), 1121−7.

(18) Ohmachi, S.; Mikami, T.; Konishi, M.; Miyake, A.; Itoh, N. Preferential neurotrophic activity of fibroblast growth factor-20 for dopaminergic neurons through fibroblast growth factor receptor-1c. *J. Neurosci. Res.* **2003**, *72* (4), 436−43.

(19) Alvarez, E.; Fey, E. G.; Valax, P.; Yim, Z.; Peterson, J. D.; Mesri, M.; Jeffers, M.; Dindinger, M.; Twomlow, N.; Ghatpande, A.; LaRochelle, W. J.; Sonis, S. T.; Lichenstein, H. S. Preclinical characterization of CG53135 (FGF-20) in radiation and concomitant chemotherapy/radiation-induced oral mucositis. *Clin. Cancer Res.* **2003**, *9* (9), 3454−61.

(20) Jeffers, M.; McDonald, W. F.; Chillakuru, R. A.; Yang, M.; Nakase, H.; Deegler, L. L.; Sylander, E. D.; Rittman, B.; Bendele, A.; Sartor, R. B.; Lichenstein, H. S. A novel human fibroblast growth factor treats experimental intestinal inflammation. *Gastroenterology* **2002**, *123* (4), 1151−62.

(21) Plotnikov, A. N.; Eliseenkova, A. V.; Ibrahimi, O. A.; Shriver, Z.; Sasisekharan, R.; Lemmon, M. A.; Mohammadi, M. Crystal structure of fibroblast growth factor 9 reveals regions implicated in dimerization and autoinhibition. *J. Biol. Chem.* **2001**, *276* (6), 4322−9.

(22) Eriksson, A. E.; Cousens, L. S.; Weaver, L. H.; Matthews, B. W. Three-dimensional structure of human basic fibroblast growth factor. *Proc. Natl. Acad. Sci. U.S.A.* **1991**, *88* (8), 3441−5.

(23) Zhu, X.; Komiya, H.; Chirino, A.; Faham, S.; Fox, G. M.; Arakawa, T.; Hsu, B. T.; Rees, D. C. Three-dimensional structures of acidic and basic fibroblast growth factors. *Science* **1991**, *251* (4989), 90−3.

(24) Fan, H.; Ralston, J.; Dibiase, M.; Faulkner, E.; Russell Middaugh, C. Solution behavior of IFN-β-1a: An empirical phase diagram based approach. *J. Pharm. Sci.* **2005**, *94* (9), 1893−911.

tive polyanions on the protein's thermal stability are further evaluated using far-UV CD, intrinsic fluorescence spectroscopy, and differential scanning calorimetry (DSC) in an attempt to relate the properties of this protein to other members of the FGF family.

Experimental Section

Materials. Highly purified recombinant FGF20 (CG53135) was provided by CuraGen Corp. with a purity of >95% as determined by SDS−PAGE. Sucrose octasulfate potassium salt was obtained from Toronto Research Chemicals Inc. (Toronto, ON). All other chemicals were purchased from Sigma (St. Louis, MO).

Sample Preparation. The stock FGF20 samples were dialyzed against 10 mM phosphate/10 mM citrate buffer containing 200 mM sodium sulfate at pH 4.5, 5.0, 5.5, 6.0, 7.0, and 8.0. FGF20 exhibits limited solubility and stability in aqueous solution. On the basis of previous results and also since it is CD transparent, sodium sulfate was added to stabilize the protein and to increase its solubility, allowing protein concentrations sufficiently high to produce adequate spectroscopic signals. Dialysis was performed overnight with one 2 L buffer change. Gross precipitation of FGF20 was observed during dialysis at pH 3−5.5, and therefore, the protein was not studied over that pH range. The dialyzed samples were filtered through a 0.45 μm low protein-binding filter (MILLEX-HV, Millipore) to remove insoluble aggregates. The samples were diluted accordingly after dialysis so that the final concentrations of samples were approximately 0.2 mg/mL. The protein concentration was determined using an experimentally determined extinction coefficient ($E^{0.1\%}_{1cm}$) of 0.97 at 280 nm.

Derivative UV Absorbance Spectroscopy. UV absorbance spectra of FGF20 were collected as a function of temperature from 10 to 80 °C with an Agilent (Palo Alto, CA) 8453 UV−visible spectrophotometer at 2.5 °C intervals. The samples were allowed to equilibrate at each temperature for 5 min (sufficient for equilibrium to be reached) with an integration time of 25 s. The optical density at 350 nm was monitored as a function of temperature in an effort to study the aggregation behavior of the protein. Derivative data analysis was performed with HP UV-Visible Chemstation. Initial attempts to obtain the second-derivative spectra by fitting the data to a third-order polynomial with a nine-point Savitzky−Golay filter were made. The data were smoothed using 99 interpolated points between each raw data point, and the negative absorption peaks were identified using Origin 6.0. Due to severe aggregation, the data at high temperatures are quite noisy and peak positions cannot be unambiguously identified in the second-derivative spectra. Therefore, fourth-derivative spectra were obtained using the same process except the data were fit to a fifth-order polynomial and the positive peaks were monitored. Resolution of the spectra is much enhanced using the fourth-derivative analysis. Seven absorption peaks resulting from the various aromatic residues were followed throughout the entire temperature range.

Fluorescence Spectroscopy. Fluorescence spectra of FGF20 were obtained employing a PTI (Monmouth Junction, NJ) Quanta Master spectrofluorometer, equipped with a Peltier temperature-controlled four-cell sample holder. Quartz cuvettes with a path length of 1 cm were used, and the slit width for both excitation and emission was set at 4 nm. The Trp fluorescence was monitored with an excitation wavelength of 295 nm, and emission spectra were collected over a wavelength range of 305−440 nm. To eliminate interference by residual light scattering, a 309 nm filter was used on the emission monochromator. For extrinsic ANS fluorescence experiments, an optimal molar ratio of 20:1 (ANS:protein) determined by preliminary titration experiments was used. The samples were excited at 375 nm, while the emission spectra were collected from 400 to 600 nm. The weak emission spectrum of ANS in buffer alone was subtracted as a blank. Both Trp and ANS fluorescence emission spectra were collected from 10 to 80 °C at 2.5 °C intervals with a 5 min equilibration time at each temperature point. The emission peak wavelength was determined using a "center of spectral mass" method, which locates peak positions at a wavelength somewhat higher than that of the actual spectra but produces enhanced reproducibility.

Circular Dichroism. Far-UV CD studies were performed with a Jasco (Tokyo, Japan) 810 spectrophotometer using cells with a path length of 0.1 cm. CD spectra were collected from 195 to 260 nm under all pH conditions using a scanning speed of 10 nm/min and a resolution of 0.1 nm at 10 °C. The CD signals at 207 and 227 nm were monitored as a function of temperature from 10 to 80 °C for samples at pH 5−8, with a resolution of 0.5 °C and a heating rate of 15 °C/h.

Empirical Phase Diagrams. Data from the fourth-derivative UV absorption spectra (seven absorption peaks) were first used to generate a phase diagram from pH 4.5 to 8. Far-UV CD (molar ellipticities at 207 and 227 nm) and intrinsic fluorescence (emission peak positions) data were also used to generate a phase diagram only from pH 5 to 8, since the sample concentration and light scattering problems at pH 4.5 were not sufficient for CD and fluorescence measurements. All mathematical analyses involving vector and matrix operations were performed using Matlab (The Mathworks Inc., Natick, MA). Details concerning the theory and mathematical analysis can be found elsewhere.[24,25] Basically, the experimental data are first converted into a number of *N*-dimensional vectors in a temperature−pH phase space, with one vector generated at each specific combination of pH and temperature. The dimension of the vectors, *N*, refers to the number of variables included in the calculation (i.e., number of different types of data). An $N \times N$ density matrix is then generated to combine the resultant multidimensional vectors. The vectors are subsequently truncated

(25) Kueltzo, L. A.; Ersoy, B.; Ralston, J. P.; Middaugh, C. R. Derivative absorbance spectroscopy and protein phase diagrams as tools for comprehensive protein characterization: A bGCSF case study. *J. Pharm. Sci.* **2003**, *92* (9), 1805−20.

into a smaller dimension (typically three) on the basis of their eigenvectors and corresponding eigenvalues determined from the density matrix. The resultant three-dimensional vectors are converted into a color plot in the corresponding temperature−pH region using an arbitrary color system of red, green, and blue. Regions of similar colors represent pH and temperature ranges within which the structural data of the protein are substantially coherent.

Effect of Polyanions. Heparin, phytic acid (inositol hexaphosphate), and sucrose octasulfate (SOS) were used as representative compounds to study the effect of polyanions on the thermal stability of FGF20. Each of these solutes was used at a concentration of 50-fold weight excess (solute: protein, w/w) in a pH 7, 100 mM phosphate buffer. A protein concentration of 0.2 mg/mL was used for all the experiments described below.

The same instrument and experimental procedure that are described above were used for CD analysis. Intrinsic fluorescence spectra of FGF20 in the presence and absence of polyanions were collected using a Jasco FP-6500 spectrofluorometer. The samples were excited at 280 nm, and emission spectra were collected from 295 to 400 nm. Emission spectra were collected from 10 to 80 °C at 2.5 °C intervals with a 5 min equilibration time at each temperature point. Spectra of buffers containing different polyanions were also collected and subtracted from the sample spectra as blanks. The center of spectral mass method was also used to determine the fluorescence emission maximum.

DSC thermograms were collected with a VP-DSC device from Microcal LLC (Northampton, MA). Thermograms were recorded from 10 to 90 °C at a scan rate of 1 °C/min under a pressure of 25 psi. Buffers containing different polyanions were also scanned, and these thermograms were subtracted from the corresponding sample data as blanks. The data were converted into molar heat capacity, and transition temperatures were determined using Microcal Origin. Further thermodynamic analysis was not attempted due to the irreversibility of the observed transitions.

Results

Aggregation of FGF20. FGF20 aggregates and precipitates from solution under acidic pH conditions. As mentioned above, gross precipitation of FGF20 is observed during dialysis at pH 3−5.5, with little protein remaining in solution at pH 3−4.5. The optical density of FGF20 solutions at 350 nm (OD_{350}) was measured to monitor the protein's aggregation behavior induced by temperature increases between pH 5 and 8. As shown in Figure 1, increases in optical density at high temperatures can be related to increased particle size due to aggregation, while a later drop in the signal reflects gross precipitation (settling) of the protein. The heat-induced aggregation behavior of FGF20 is strongly pH dependent. At pH 5, the maximum OD_{350} is observed at ∼46 °C, which increases to 52 °C at pH 5.5 and further to ∼60 °C at pH 6−8. At pH 5, the increase in OD can be detected as low as 30 °C.

Tertiary Structure of FGF20. The intrinsic fluorescence of the single Trp residue in FGF20 was monitored as a probe for tertiary structure changes. The actual emission maximum of 329 nm was observed for FGF20 over the entire pH range of 5−8 at 10 °C, suggesting no change in the microenvironment of the Trp residue over this pH range. The Trp emission peak position is plotted as a function of pH and temperature in Figure 2A. Note the peak position data presented in the plot are determined by a center of spectral mass method. The emission maximum wavelengths determined by this method are approximately 14 nm higher than the actual values (i.e., 329 nm at 10 °C). This method is used, however, due to the better precision of the final data. The trends in peak position changes as a function of temperature are still described well by this approach. The emission maximum shifts to a higher wavelength after the conformational change, suggesting an increased level of exposure of the single Trp residue to the solvent. Effects of pH on the thermal transition temperature of FGF20 similar to those detected in turbidity measurements and derivative UV absorption analysis are observed (see below), with pH 5 manifesting the transition at the lowest temperature (near 40 °C).

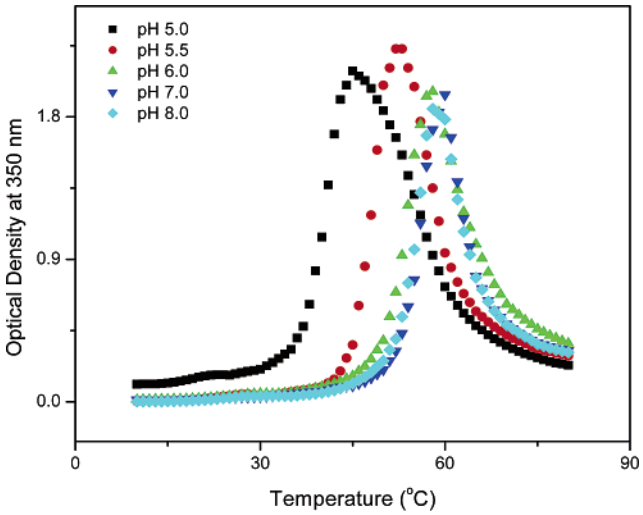

Figure 1. Aggregation behavior of FGF20. Optical densities at 350 nm (OD_{350}) are recorded as a function of temperature for FGF20 at pH 5−8.

ANS binds primarily to apolar sites on proteins, which often results in an increase in the dye fluorescence intensity and a shift of its emission maximum to a lower wavelength. Electrostatic interactions may also be involved in the binding since ANS molecules are negatively charged. Figure 2B illustrates ANS fluorescence intensities at its emission maximum as a function of pH and temperature. A temperature-induced transition was detected at all pH values, with ANS fluorescence intensity increasing at the transition. Thus, FGF20 appears to undergo a conformational change as the temperature increases, exposing apolar binding sites. The transition temperatures detected with ANS fluorescence are several degrees lower than those determined by the other techniques. A pH dependence similar to that of the transition temperatures, however, is still observed.

High-resolution derivative UV absorption spectroscopy monitors changes in the microenvironment of all three

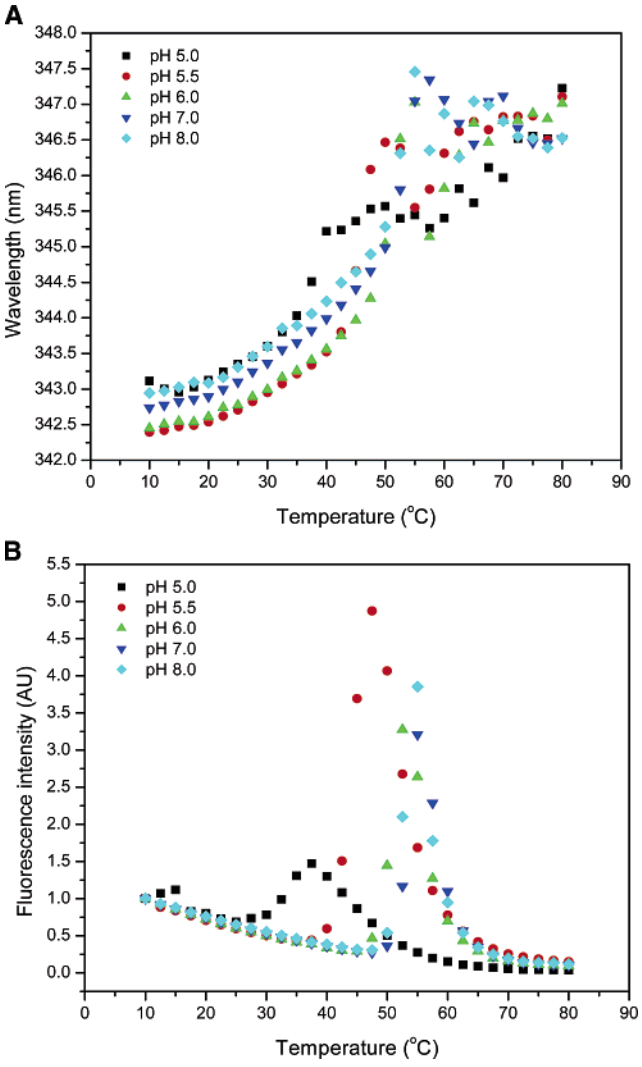

Figure 2. Intrinsic and extrinsic fluorescence of FGF20. Trp fluorescence emission peak positions of FGF20 at pH 5−8 are plotted as a function of temperature (A). The excitation wavelength is set at 295 nm (>95% Trp fluorescence). Emission peak positions are determined by a center of spectral mass method. ANS fluorescence intensities at 480 nm of FGF20 are plotted as a function of temperature (B). A molar ratio of 20:1 ([ANS]:[protein]) and an excitation wavelength of 372 nm were used. Data are normalized to the intensity at 10 °C at each pH value.

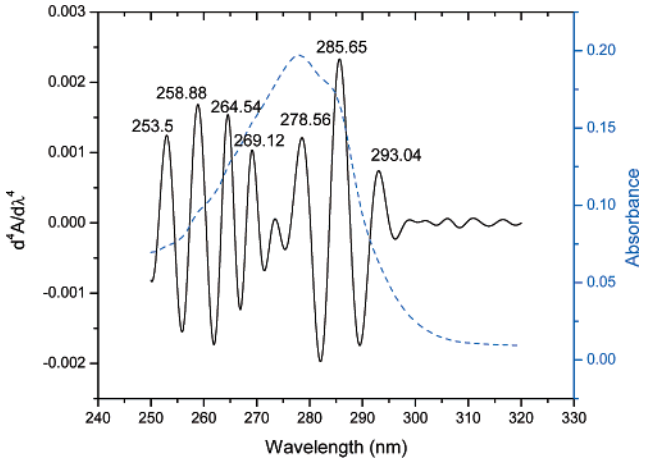

Figure 3. Representative UV absorbance spectrum of FGF20 (– – –) and its fourth derivative (—). Seven individual absorption peaks are resolved as positive peaks in the fourth-derivative spectra. The spectrum was obtained at a protein concentration of 0.2 mg/mL at 10 °C and pH 7.

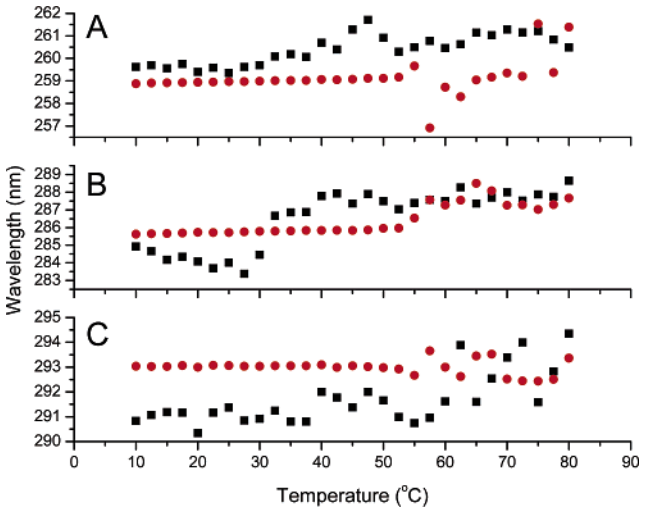

Figure 4. Fourth-derivative UV absorption spectroscopy analysis of FGF20. Absorption peak positions around 259 (Phe, A), 285 (Tyr/Trp, B), and 293 nm (Trp, C) for FGF20 at pH 4.5 (squares) and pH 7 (circles) are plotted as a function of temperature. Significant shifts in peak positions are observed with these three peaks at low temperatures between pH 4.5 and 7.

aromatic residues, providing a more global picture of the behavior of the tertiary structure than intrinsic fluorescence since these residues are dispersed throughout the protein's structure. Structural changes of the protein can be probed by monitoring shifts in the individual absorption peaks resolved by derivative analysis.[26] In this case, to better resolve each individual absorption peak, fourth-derivative absorption spectra were obtained instead of the more commonly used second-derivative analysis. As illustrated in Figure 3, seven positive peaks were identified corresponding to Phe (253, 259, 264, and 269 nm), Tyr (278 nm), Tyr/Trp (285 nm), and Trp (293 nm). The wavelength positions of these peaks are followed as a function of pH and temperature to detect potential conformational changes of the protein. A major effect of pH on peak position was observed at pH 4.5 compared to the other pH conditions examined at 10 °C (Figure 4). A peak shift of ~0.5 nm is observed with the peaks at 259 and 285 nm, while the Trp peak at 293 nm exhibits an even larger change of nearly 2 nm. This suggests a large alternation in the tertiary structure of FGF20 below pH 5. Significant changes in peak position were also observed at elevated temperatures due to temperature-induced

(26) Mach, H.; Volkin, D. B.; Burke, C. J.; Middaugh, C. R. Ultraviolet absorption spectroscopy. *Methods Mol. Biol.* **1995**, *40*, 91−114.

conformational changes and subsequent aggregation of the protein. Gross precipitation of the protein causes the data to become very noisy after the major transition. These data are better summarized using the empirical phase diagram approach described below.

Secondary Structure of FGF20. The far-UV CD spectra of FGF20 manifest a positive peak at 227 nm and a negative signal near 207 nm (Figure 5A), which is typical for proteins of the FGF family.[4] Other proteins that have extensive β-trefoil structure such as hisactophilin also share the spectral feature at 205−208 nm.[27] Presumably, the positive peak at 227 nm arises from aromatic residues and reflects specific tertiary structure features of the protein, while the secondary structure component produces the β-like negative signal at 207 nm.[28,29] At elevated temperatures, a broad minimum near 216 nm was observed with the CD spectra of FGF20. This may reflect the presence of intermolecular β-sheet formed during protein association at high temperatures. The CD signals at 207 and 227 nm were both monitored as a function of temperature at different pH values (Figure 5B,C). A major temperature-induced transition is seen, accompanied by precipitation of the protein. A significant decrease in the magnitude of the CD signals is observed at both wavelengths throughout the entire pH range that was examined. There is no significant difference between the transition temperatures determined at these two different wavelengths. The protein at pH 5 appears to be the most labile with a melting temperature of ∼40 °C.

Empirical Phase Diagram. To better summarize the behavior of FGF20 under the pH and temperature conditions that were investigated, an empirical phase diagram was constructed from pH 4.5 to 8 using data from fourth-derivative UV absorption spectra (the seven positive peak positions were used as the initial seven components in vectors). As illustrated in Figure 6A, two phases can be identified in the low-temperature region. A major phase corresponding to presumably the native state of the protein exhibits a unified green region from pH 5 to 8. A second phase exists at pH 4.5 from 10 to 30 °C, suggesting the altered structure of FGF20 under these conditions. A major temperature-induced conformational change causes the protein to aggregate at elevated temperatures, which leads to the third phase with varied colors. Gross precipitation of FGF20 causes the solution to be less homogeneous, and the absorption peak position data are quite noisy, which leads to the color dispersion phenomenon observed in this phase.

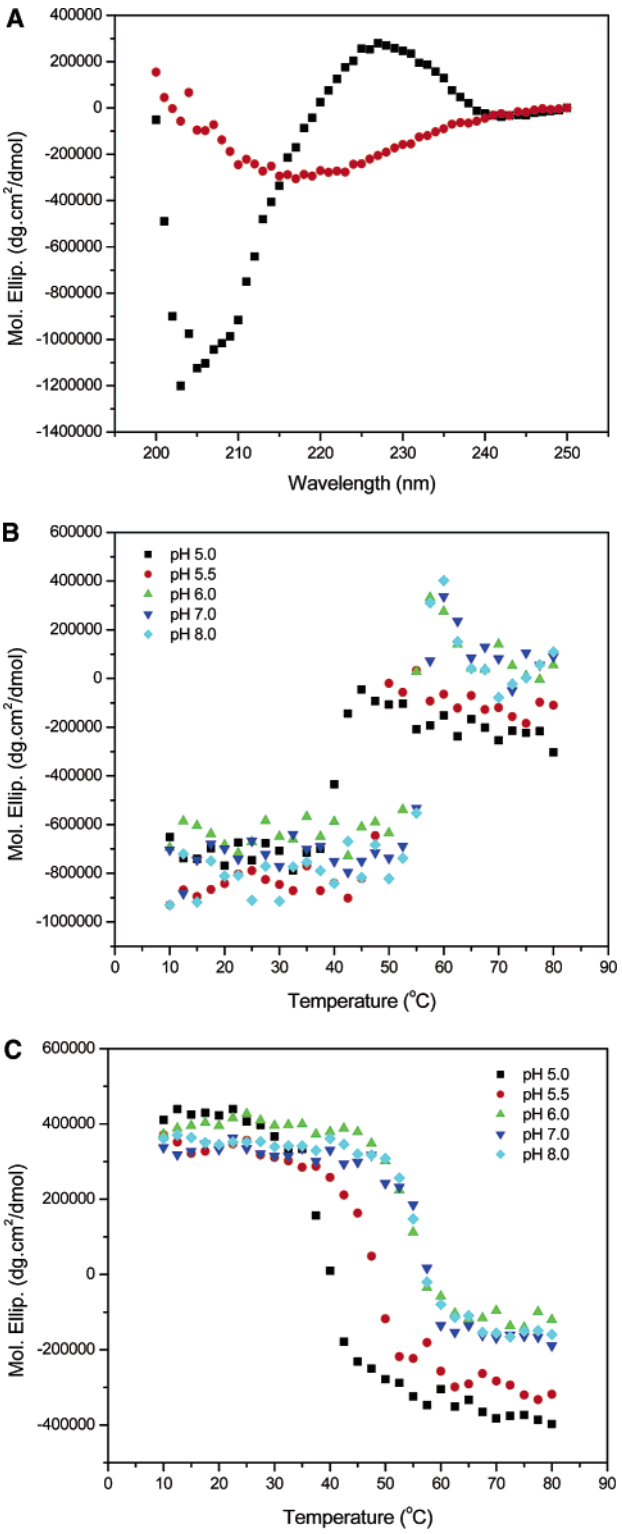

Figure 5. Far-UV CD analysis of FGF20. CD spectra of FGF20 (A) at pH 7 are recorded at 10 (squares) and 70 °C (circles). CD signals of FGF20 at 207 (B) and 227 nm (C) are measured as a function of temperature. There is no significant difference between the transition temperatures determined at these two different wavelengths.

The phase transition temperatures, at which abrupt color changes occur in the phase diagram, indicate the relative

(27) Liu, C.; Chu, D.; Wideman, R. D.; Houliston, R. S.; Wong, H. J.; Meiering, E. M. Thermodynamics of denaturation of hisactophilin, a β-trefoil protein. *Biochemistry* **2001**, *40* (13), 3817−27.
(28) Woody, R. W.; Dunker, A. K., Aromatic and Cystine Side-Chain Circular Dichroism in Proteins. In *Circular Dichroism and the Conformational Analysis of Biomolecules*; Fasman, G. D., Ed.; Plenum Press: New York, 1996; pp 109−58.
(29) Venyaminov, S. Y.; Yang, J. T. Determination of Protein Secondary Structure. In *Circular Dichroism and the Conformational Analysis of Biomolecules*; Fasman, G. D., Ed.; Plenum Press: New York, 1996; pp 69−109.

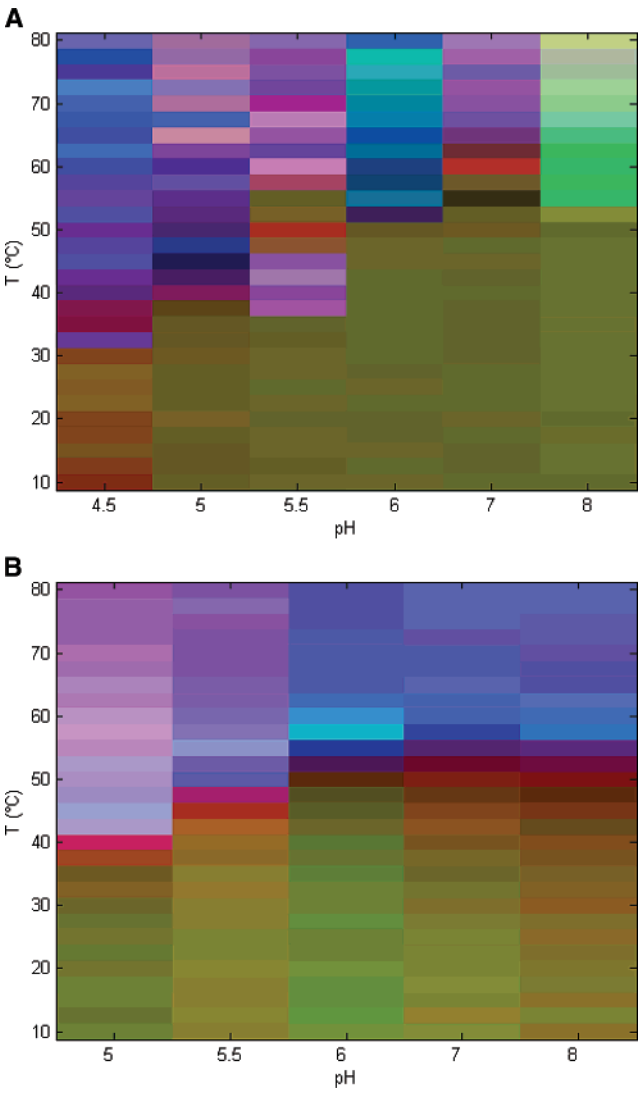

Figure 6. Empirical phase diagrams of FGF20. Empirical phase diagrams of FGF20 at pH 4.5−8 are first constructed from UV absorption spectroscopy data using the seven absorption peaks resolved by derivative analysis (A). Two phases are observed in the low-temperature region at pH 4.5 and 5−8. A second phase diagram at pH 5−8 (B) is constructed using CD (signals at 227 and 207 nm) and intrinsic fluorescence (emission peak wavelength) data. Two major phases at low and high temperatures are resolved. Empirical phase boundaries are clearly seen as the temperature and pH are varied. FGF20 at near-neutral pH exhibits the highest thermal stability.

thermal stability of the protein at different pH values. The greatest thermal stability is observed near neutral pH.

Data from CD (molar ellipticity at 207 and 227 nm) and intrinsic fluorescence (emission maximum) experiments were used to generate a second phase diagram from pH 5 to 8 (Figure 6B). This includes information about both the secondary and tertiary structure of the protein. Two major phases with more uniform color are resolved using this approach. The pH dependence of the transition temperature is again well defined, with phase boundaries detected near 40 °C at pH 5, 48 °C at pH 5.5, and up to 52 °C at pH 6−8.

Effect of Polyanions. The effects of polyanions on the conformation and thermal stability of FGF20 were first examined using far-UV CD and intrinsic fluorescence spectroscopy. Heparin is used as a typical high-molecular mass polyanion, while phytic acid and sucrose octasulfate (SOS) are used as representative low-molecular mass polyanions. All solutes were used at a concentration of 50-fold weight excess (solute:protein, w/w) in a pH 7, 100 mM phosphate buffer. No apparent effects of these solutes on the native conformation of FGF20 were observed on the basis of CD and fluorescence experiments. As illustrated in panels A and B of Figure 7, the presence of phytic acid and SOS causes the apparent T_m to increase by only 3−4 °C, while a much greater stabilizing effect is observed in the presence of heparin. In the fluorescence experiments, the decrease in the emission maximum observed at high temperatures may reflect the increased light scattering caused by aggregation and precipitation of FGF20.

DSC was also used to study the effects of these polyanions on the thermal stability of FGF20. As illustrated in Figure 7C, the DSC thermogram of FGF20 exhibits a broad endothermic transition followed by an exothermic signal corresponding to aggregation and precipitation of the protein. The presence of polyanions significantly enhances the thermal stability of FGF20, with heparin exhibiting the greatest increase in T_m (∼12 °C). An increase of approximately 1.5 °C is also observed when the buffer concentration increases from 50 to 100 mM phosphate, presumably due to either the stabilizing effect of phosphate ions as polyanions or perhaps the increased ionic strength.

Discussion

Structure of FGF20. FGF20 is a 23 kDa protein of 211 amino acid residues. It is expected to exhibit structural features similar to those of FGF9 on the basis of their sequence homology. The secondary structure of FGF20 appears to be dominated by β-sheet. Far-UV CD spectra of FGF20 exhibit features typical for proteins containing β-trefoil structure, which appears to be a common feature of the FGF family. The necessary presence of sodium sulfate in these studies causes the CD spectra below 205 nm to not be resolvable, preventing an estimate of the amount of each secondary structural component using computational methods. In contrast to that of FGF1 and some other members of the FGF family, the intrinsic fluorescence of the single Trp residue in FGF20 is not quenched in its native state, with significant fluorescence intensity detected when the Trp residue is selectively excited at 295 nm. The Trp residue appears to sit in a different environment compared to that in FGF1, which is confirmed by structure-based sequence alignment among FGF1, FGF9, and FGF20, as well as the lack of a quenching His residue in FGF20.[16,21] Similar to FGF9, FGF20 also appears to exist as a dimer, exhibiting an approximate molecular mass of ∼46 kDa (not illustrated).

Effects of pH, Temperature, and Polyanions. Like other FGF family members, FGF20 appears to be unstable at acidic pH. Adjusting the solution pH to values below 5 causes

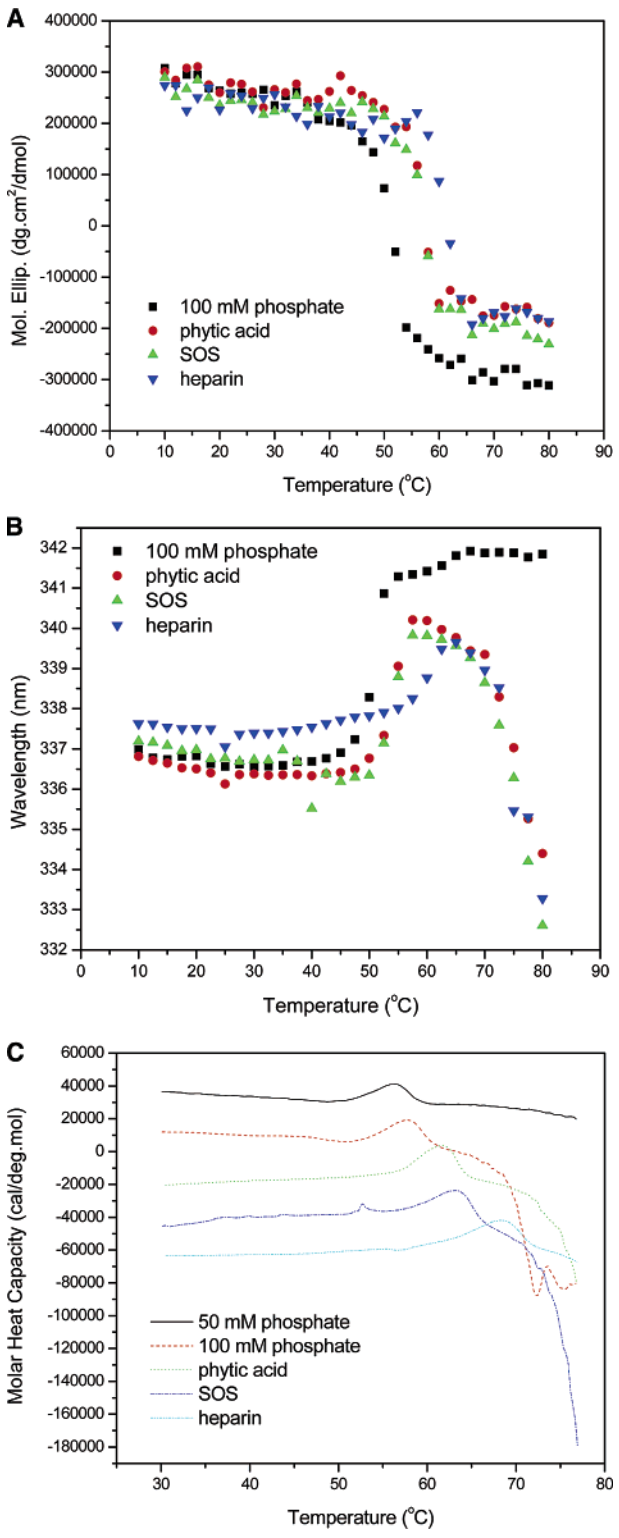

Figure 7. Effects of polyanions (phosphate, phytic acid, sucrose octasulfate, and heparin) on the thermal stability of FGF20. Effects of polyanions on the thermal stability of FGF20 at pH 7 are examined by CD (CD signals at 227 nm, A), intrinsic fluorescence (emission peak positions, B), and DSC (C) analysis in the presence and absence of three representative polyanions (at a 50-fold weight excess of polyanins to protein). The greatest stabilizing effects are observed in the presence of heparin.

severe aggregation and precipitation of the protein. No effect of pH on the native structure of FGF20 is observed from pH 5 to 8. FGF20 exhibits a major temperature-induced structural transition followed by protein aggregation. Much lower transition temperatures are observed at pH 5 and 5.5 compared to those at more neutral pH. Unlike some FGF family members, FGF20 exhibits a transition temperature significantly above physiological temperature under the conditions of this study. A T_m of ~55 °C is seen for the protein in a pH 7, 100 mM phosphate buffer using DSC analysis.

Molten globule-like states are often observed with FGFs, in which their native secondary structure is retained while the tertiary structure is substantially altered. For example, transition temperatures of FGF1 determined by CD signal changes appear to be 5−7 °C higher than those determined from fluorescence intensity changes,[4] suggesting the presence of a molten globular state. This phenomenon is not, however, observed with FGF20 in this work. This could reflect the stabilization provided by the presence of sodium sulfate. It is also possible that the effects of severe aggregation and precipitation immediately after the initial structural change dominate the temperature-induced signal changes for both CD and fluorescence measurements, preventing differences in the apparent T_m from being unambiguously detected. Thus, partially unfolded states of FGF20 may still exist, but their detection may require additional experimental approaches.

As illustrated by CD, intrinsic fluorescence, and DSC analysis, interactions between polyanions and FGF20 can significantly enhance its thermal stability like some of the members of the FGF family. Previous studies of FGF9 suggest the presence of three potential heparin/polyanion binding sites on its surface. The first site consists of Arg180, Tyr163, and Arg 161. The three basic residues, Arg137, Lys154, and Arg161, are involved in the second site, while the third primarily contains Arg173 and Arg177.[21] All eight of these residues are conserved in FGF20[16] and form clusters of positively charged residues potentially available for interaction with polyanions.

Empirical Phase Diagram. The empirical phase diagram approach provides an intuitive way to visualize the ability of FGF20 to respond to pH and temperature. The noisy peak wavelength data from derivative analysis of absorption spectra are summarized well in the phase diagram. Structural alternations induced by a pH of <5 are manifested as a distinct color change at low temperatures. Effects of pH on the thermal stability of FGF20 are more clearly demonstrated in the phase diagram constructed using CD and fluorescence data, with empirical phase boundaries detected over different temperature ranges at different pH values. For example, unlike the phase diagram constructed from UV absorbance data, the abrupt color change observed at pH 5.5 occurs at a temperature ~8 °C higher than that detected at pH 5. These apparent phase boundaries can be further used to determine potential solution conditions in accelerated stability studies of the protein. For FGF20, a pH of ~7 and a temperature range of 45−50 °C can be chosen as initial conditions.

Techniques such as optical density and fluorescence measurements can then be easily adapted to a microtiter plate format and used to screen for potential stabilizers of FGF20. Thus, the first structural analysis of this important growth factor provides a tool for the development of pharmaceutical formulations.

MP060097H